POLITECNICO DI TORINO
Repository ISTITUZIONALE

Towards Kardashev-Scale Type I of Human Advancement in Technological Civilization: An Innovative Solar Annular System for Energy Harnessing

Original
Towards Kardashev-Scale Type I of Human Advancement in Technological Civilization: An Innovative Solar Annular System for Energy Harnessing / Safaei, A., Marazzato, B., Dalla Vedova, M.D.L., Maggiore, P.. - (2025). (AIAA Science and Technology Forum and Exposition, AIAA SciTech Forum 2025 Orlando, FL (USA) 6-10 January 2025) [10.2514/6.2025-2028].

Availability:
This version is available at: 11583/3009237 since: 2026-03-25T21:38:46Z

Publisher:
American Institute of Aeronautics and Astronautics Inc, AIAA

Published
DOI:10.2514/6.2025-2028

Terms of use:

This article is made available under terms and conditions as specified in the corresponding bibliographic description in the repository

Publisher copyright
AIAA preprint/submitted version e/o postprint/Author's Accepted Manuscript

(Article begins on next page)

18 November 2026

Towards Kardashev-Scale Type I of Human Advancement in Technological Civilization: An Innovative Solar Annular System for Energy Harnessing

Arash Safaei[1], Benedetta Marazzato[2],
Matteo Davide Lorenzo Dalla Vedova[3] and Paolo Maggiore[4]
Politecnico di Torino, Torino, 10129, Italy

The presented study introduces a novel aerospace system based on an implementation of the Dyson Sphere concept proposed by the physicist Freeman Dyson in 1960. This groundbreaking revised technology involves a constellation of satellites equipped with advanced photovoltaic panels, arranged in a seamless ring orbiting around the Earth. These satellites efficiently capture solar energy from the sun and transmit it to ground stations via wireless power transmission techniques, such as microwave or laser beaming. The whole system leverages cutting-edge materials with outstanding thermal and photovoltaic characteristics, guaranteeing minimum energy dissipation and maximum durability in the harsh space environment. Integrated control systems ensure accurate alignment and efficient energy distribution, effectively addressing the complexities of dynamic orbital mechanics. For this purpose, a dynamic model implemented through Matlab, Simulink, and Ansys is presented, capable of simulating the transient and steady-state response of the materials used in the architecture of the sample satellite designed to direct solar energy from space to Earth. This model allows for the variation of sensitive parameters of the entire architecture (from material selection to orbit type) to evaluate which combination of these parameters achieves the most efficient and effective configuration of the satellite constellation around the Earth. The validation of the dynamic model implemented on Matlab-Simulink was carried out by cross-referencing data obtained from the simulations of the scaled physical model with Ansys Speos and Ansys Thermal.

I. Introduction

The Dyson Sphere, proposed by scientist Freeman Dyson in 1960 [1], is a highly ambitious project in the fields of astrophysics and aerospace engineering. Dyson suggested that a highly developed society may construct an expansive structure around a star to harness a substantial amount of its energy production, thereby effectively addressing the issue of limited energy resources on a large scale [2]. Throughout the years, numerous designs for the Dyson Sphere have been suggested, each presenting distinct engineering obstacles and restrictions:

1) Dyson Swarm: this configuration consists of a large number of independent satellites orbiting the reference star. The primary advantage is its modularity, which enables gradual construction. Nevertheless, the obstacles include the challenge of maintaining orbital stability, evading collisions, and overseeing the immense distances between each satellite [3]

[1] PhD Student, Department of Mechanics and Aerospace Engineering (DIMEAS)
[2] MSc Student, Department of Mechanics and Aerospace Engineering (DIMEAS)
[3] Assistant Professor, Department of Mechanics and Aerospace Engineering (DIMEAS)
[4] Full Professor, Department of Mechanics and Aerospace Engineering (DIMEAS)

2) Dyson Shell: it is a more ambitious concept that involves a solid structure around a star, at a certain distance. Although it is theoretically possible to capture nearly all of a star's energy, the existing technological limitations make it impossible to overcome the engineering obstacles, which involve significant amounts of materials needed, the ability of the structure to withstand star gravitational pressure, and the management of heat generated by the captured energy [4]
3) Niven Ring: this concept describes a ring-like structure orbiting around a star. Despite being less complex than a complete shell like the Dyson's one, this design nonetheless necessitates exceptional materials and building methods to uphold structural stability and handle the substantial centrifugal forces [5]

When examined from the standpoint of aerospace, the Dyson Sphere presents several appealing advantages. According to the theory, it could potentially provide a supply of energy that is essentially limitless by catching the majority or all the radiative output of a star. The extension of a civilization across interstellar distances would be supported by this, which would give rise to the possibility of large-scale space exploration, colonization, and the development of advanced technological capabilities [6-7]. Nevertheless, the difficulties that are associated with the construction of a Dyson Sphere are significant, both in terms of the engineering requirements and the resources that must be allocated. Materials with outstanding strength-to-weight ratios, resilience to severe temperatures, and long-term durability against cosmic radiation and micrometeoroid impacts are required for the project because of its sheer magnitude, which involves a structure that may potentially span astronomical units. To control and coordinate many satellites, each of which is subject to gravitational perturbations and the possibility of collisions, it would be necessary to have autonomous systems that are well beyond the capabilities that are currently available. Though theoretically advantageous, the traditional Dyson Sphere, as it is described in literature, is therefore not only impractical but also nearly impossible to build in our modern days. This is evident from an engineering point of view as well as in terms of the amount of time that it would be necessary to build such a massive orbiting structure [8], comparable to the size of our sun. Therefore, the purpose of this study is to provide a practical concept for a Dyson Sphere that is assembled around the Earth and adapted to it, as shown in Figure 1. This would result in an orbiting structure that would no longer orbit around a star but rather around the target planet of interest. In this way, a significant reduction is achievable in both the level of complexity and the resources that are necessary for its direct implementation. To estimate and subsequently implement a constellation of satellites that are capable of continuously transmitting energy from space to Earth, it is necessary to place in precise orbits enough satellites that can capture solar radiation and transmit it to the ground stations via microwaves and radiofrequency [9-10]. Additionally, it is necessary to appropriately orient these satellites so that they are always facing the sun while pointed at ground rectennas that have been placed in suitable locations on Earth. To this end, a mathematical and physical model has been developed to simulate the dynamic behavior of the presented architecture. Such a model is parametric, and as a result, it can handle and trigger certain input variables into the global system. These variables include the type of materials that are used in the sensitive parts of the satellite, the orientation of the surfaces, the type of orbit, the efficiencies of the various subsystems, and many others.



Fig. 1 Artistic representation of the Dyson Sphere around the Earth and the Sun.

The output of the model is then integrated with the results of thermal simulations performed using Ansys Thermal Transient, optical simulations with Ansys Speos, and orbital simulations carried out using the Aerospace and Satellite Communication Systems toolbox implemented in Matlab. The results of these simulations are used as input data for the Simulink model, which enables the mathematical model to be calibrated and validated based on the matching results obtained by the model itself and the performed simulations through the reported dedicated software.

II. Space-Based Solar Power Satellites: State of the Art

Space-Based Solar Power Satellites (SBSP) are sophisticated aerospace systems [11-13] engineered to harvest solar energy in space and transmit it wirelessly to Earth via microwave or laser beams [14-15], providing a sustainable energy source free from terrestrial constraints, such as the weather or visibility attenuation [16].

The SPS was initially proposed by Peter Glaser in 1968 [17], shortly followed by studies conducted by NASA and the Department of Energy [18] in the 1970s. After the initial experiments in the United States, other varieties of SPSs have been proposed. Generally, they are classified into five categories based on the utilization of the sunlight-concentrating mirror and the method of power collection and distribution [19], as illustrated in Figure 2.

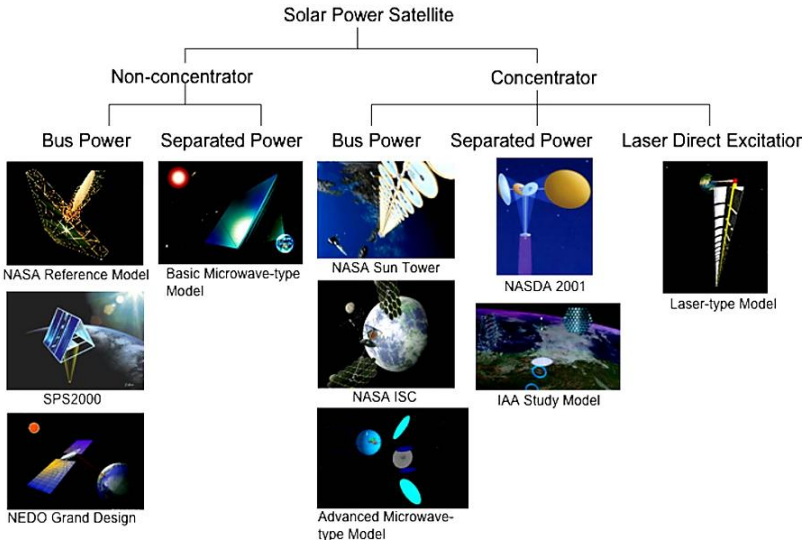


Fig. 2 Different types of SPS configurations, divided into Non-concentrator and Concentrator [20].

As can be noted, SBSP systems typically consist of large solar collectors or photovoltaic arrays placed in geostationary or other orbital configurations. The collected solar energy is converted into electrical energy and transmitted to Earth via wireless beams, where it is captured by ground-based rectennas [21-22] and then converted back into electrical energy. Wireless power transmission and reception ground stations constitutes an additional process to be considered compared to terrestrial solar power plants; however, the anticipated power loss during microwave power transmission from orbit to the reception on ground is projected to be under 50% (while nowadays the overall system conversion efficiency is around 35-38% [23]), taking into account the conversion efficiency between direct current and radio frequency, as well as propagation attenuation. To have a direct comparison between SPS and terrestrial solar power plants, it is sufficient to consider that the average solar power available per unit area in space is on average 5 to 10 times greater than that available on the Earth's surface. For instance, the average solar radiation reaching ground in the USA during the hottest month of the year is approximately 240 W/m² [24], whereas in a geosynchronous orbit, it remains constant at roughly 1367 W/m². Choosing a geostationary orbit at around 36.000 kilometers altitude for the SPS enables nearly continuous power acquisition from space year-round. The energy payback period for a 1-GW class Space Power System (SPS) is projected to be less than 10 years [25], although its operational lifespan is anticipated to exceed ten years. The operational lifespan of spacecraft is frequently constrained by the durability of solar cells in the space environment, which goes from 10 to 15 years on average [26-27], whereas radiation-resistant cells, such as copper indium selenide (CIS), exceed 30 years. By taking into consideration all the aforementioned factors, along with data collected during these recent years on the performances and assessments on the SPSs, one of the most recent types of configurations among the ones reported in Figure 2 is addressed, analyzed and implemented in this study, which is the RD1 (Representative Design One) design proposed by Mankins [28] during the 72nd International Astronautical Congress held in 2021, schematically reported in Figure 3.

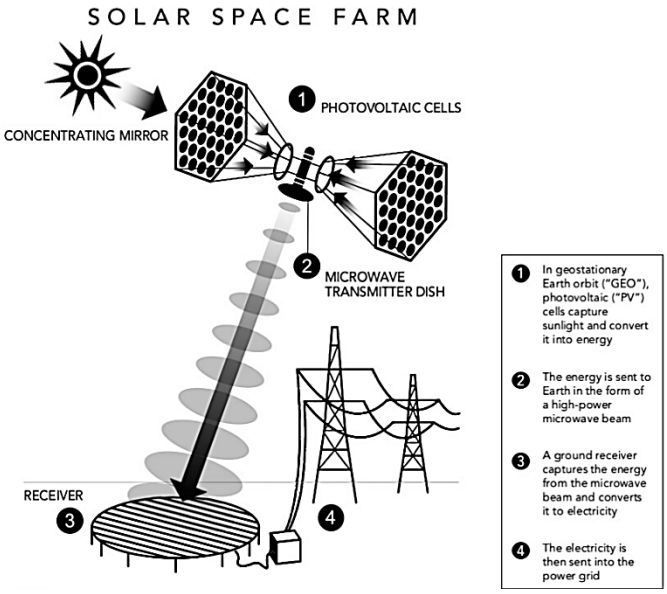


Fig. 3 Demonstration plant to capture solar radiation in GEO orbit and beaming power via wireless transmission to receiver stations on Earth [28].

Since its geometry is relatively straightforward and reproducible from both an engineering and a virtual point of view, and the presence of enough data from which to perform an exhaustive analysis, this configuration is therefore selected since it enables direct simulations to be performed on the 3D model that has been created for the purpose of this work.

III. The Solar Annular System: A Practical Solution

The architecture of the Solar Annular System proposed in this work addresses the aforementioned limitations by implementing and adapting a new concept of Dyson Sphere in a more feasible and practical design from the engineering point of view. In contrast to what is shown in Figure 1, the new system is no longer built in such a way that it completely encircles the surface of the entire planet. The traditional Dyson Sphere is thus revisited and adapted to an orbiting constellation of satellites around the Earth that takes the form of rings on well-chosen orbits.

Each satellite of the system is equipped with cutting-edge solar panels [30-31], which are feasible to withstand the space environment guaranteeing the longest possible life to the structure, with the actually achievable conversion efficiencies. Since the implemented mathematical model is parametric, it is therefore able to accept the selection of various technologies as input. This allows it to compare the outcomes of various configurations and combinations of the materials that are chosen to simulate the heat loads, thermal transients and final power flux received by the ground station.

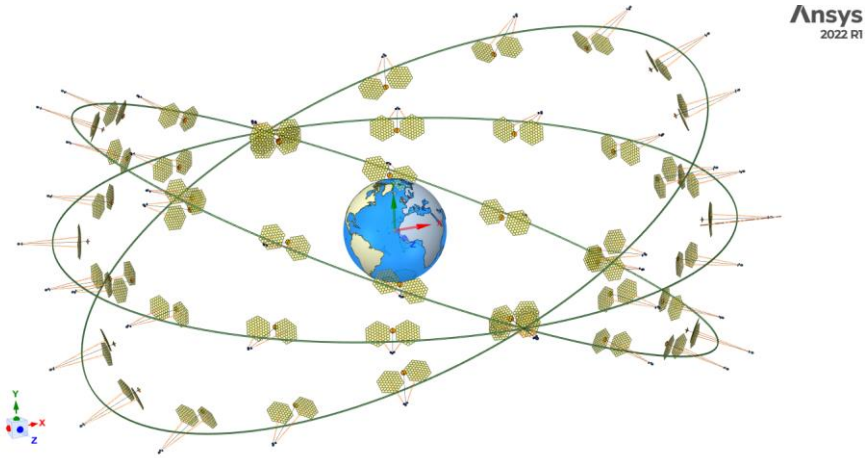


Fig. 4 Scaled 3D CAD model to be simulated through the developed mathematical model.

A. The Physical Model

The global system to be modeled is mainly made up of 3 bodies: the Sun, the Earth, and the Solar Annular System, schematized in the implemented 3D CAD model reported in Figure 4 in a configuration reporting three orbiting rings, one positioned in a geostationary orbit and two on a geosynchronous one. Constructing and simulating the 3D model at a 1:1 scale relative to real dimensions, while preserving the geometric fidelity and spatial resolution of each system component, is both computationally demanding and minimally beneficial for visual demonstration. Therefore, the model is created at the largest scale permissible by Ansys Space Claim software to maximize geometric representation and minimize scaling errors. The mathematical model replicates the system's genuine physics by considering the true dimensions of its components, while the implemented 3D models are consistently maintained at a reduced size, preserving the real proportions among the various entities. The Solar Annular System consists of several key subsystems, each designed to optimize energy collection, conversion, transmission, and structural stability in the space environment. Each satellite of the system relies on the following components [32] (schematized in Figure 5):

1) Solar Energy Collection Subsystem: its function is to capture sunlight for energy generation through large arrays of photovoltaic (PV) cells or solar concentrators, which directly receive the power flux from the Sun and redirect it toward the solar cells.
2) Power Management and Conversion Subsystems: these systems convert solar energy into a form suitable for transmission. The step needed for this conversion involves the direct current (DC) transformation from PV cells into high-frequency AC or microwave energy, which is better indicated for long distance transmissions with lower overall losses.
3) Wireless Power Transmission Subsystems: the main function is the transmission of converted energy to Earth, in the form of microwave or laser beam.
4) Structural Support and Deployment Subsystems: they ensure the satellite's structural integrity and facilitate deployment. The preferred materials are lightweight ones (e.g., carbon composites) for trusses.
5) Thermal Management Subsystems: the main goal to extend the durability of the whole satellite is to be able to regulate the temperature of the critical components to prevent overheating. Radiators and advanced coatings can be used to dissipate and reduce thermal absorption.
6) Attitude Control and Orbit Maintenance Subsystems: needed to maintain precise orientation and position of each satellite.
7) Communication and Control Subsystems: they manage satellite operation and relay data to Earth while providing real-time telemetry, command reception and beam guidance.
8) Earth Receiver Subsystems: ground-based infrastructure aimed to receive and convert transmitted energy from space segment. The main components are rectennas for microwave reception and conversion systems to supply grid-compatible electricity.

Despite the presence of several subsystems, the sensitive variables of above-mentioned systems are included as input parameters in the implemented model, to make the model flexible and adaptable to other types of architectures and operational scenarios. The possibility of modifying certain input parameters also allows for a sensitivity analysis on the entire structure to assess the weight of each initial variable on the final outputs of the architecture, such as the number of orbiting satellites and the power flow received by the ground station. Such a sensitivity analysis is not addressed in this work but is merely mentioned along with the final results.

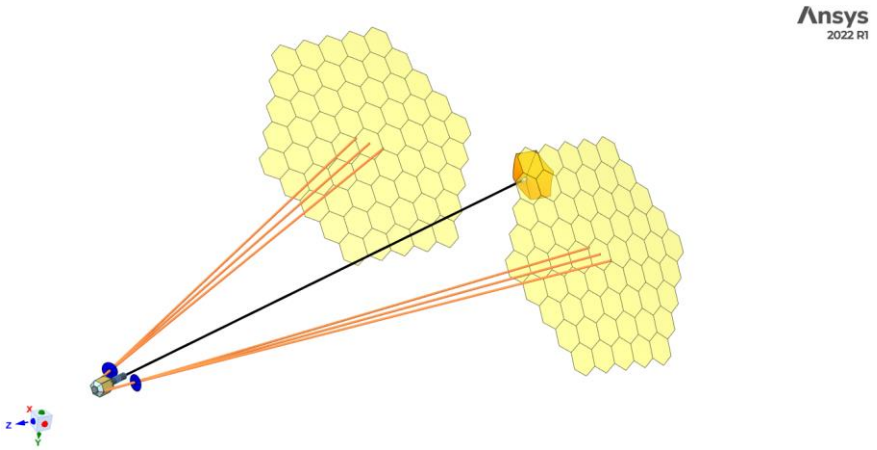


Fig. 5 3D CAD model of the implemented RD1 SPS configuration.

Once all the components of the global system are defined, including both the orbital segment and the receiving ground stations on the Earth, the whole system is then modeled through simple geometrical designs to simulate the thermal behavior and performance of the structure. The schematized diagram of the implemented thermal problem is reported in Figure 6, which considers the most important power fluxes governing the physics of the presented configuration.

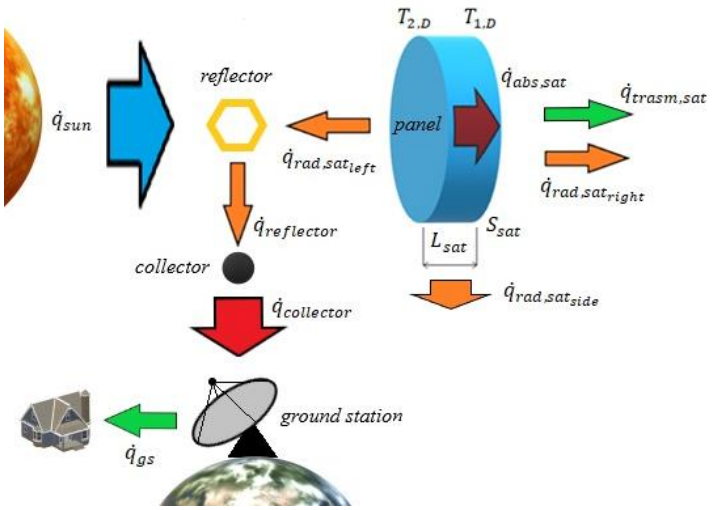


Fig. 6 Schematic representation of the thermal problem.

As can be noted from the reported diagram, each component of the system is discretized as a simple geometry, to simplify the mathematical formulation while keeping the global model as much representative as possible of the physics of the real system. The aim of the mathematical model implemented in Matlab and Simulink is not to cover every minor detail of the three-dimensional model, but to deliver a realistic representation of the physics involved, which is more easily solved and requires less time than a comprehensive three-dimensional simulation. The model is then augmented by incorporating 3D effects as input data via simulations conducted with Ansys, hence strengthening the model's physics.

B. The Mathematical Model

In the analysis and study of the power fluxes governing the whole system, all forms of heat transfer as well as the losses must be taken into consideration, to be able to express the total amount of power absorbed and released by each satellite of the Solar Annular System. Among the final outputs of the system, the most important are the power flux received by the ground stations and the number of satellites needed to fulfil the Earth global power consumption, which represents the input of the problem. This final value, along with the dimensions of each satellite's panel, will determine the overall dimension of the rings and their number around the planet needed to close the problem. With reference to Figure 6, the system of equations that describes the whole thermal problem is reported in Eq. (1), where $\dot{q}_{sun}$ is the solar constant, $\dot{q}_{abs,sat}$ the power flux absorbed by the satellite's mirrors, $\dot{q}_{trasm,sat}$ the power flux transmitted across the mirrors' panels, $\dot{q}_{refl,sat}$ the global power flux reflected by the mirrors, $\dot{q}_{refl,sat_{left}}$ the power flux reflected by the side of the mirrors directed towards the sun, $\dot{q}_{refl,sat_{right}}$ the power flux reflected by the side directed towards the earth, $\dot{q}_{refl,sat_{side}}$ the power flux reflected by the side of the mirrors toward the free space, $\dot{q}_{rad,sat_{left}}$ the power flux irradiated from the mirrors toward the collector, $\dot{q}_{rad,sat_{right}}$ the power flux irradiated from the mirrors toward the earth, $\dot{q}_{rad,sat_{side}}$ the amount of power lost due to irradiation through the sides of the panels, $\dot{q}_{reflector}$ the power flux coming from the mirrors and reflected back toward the collectors, $\dot{q}_{collector}$ the power flux directed toward the collectors of the photovoltaic panels, $\dot{q}_{trasm,coll}$ the power flux transmitted across the collector, $\dot{q}_{abs,coll}$ the power flux absorbed by the collector, $\dot{q}_{refl,coll}$ the global power flux reflected by the collector, $\dot{q}_{refl,coll_{left}}$ the power flux reflected by the left side of the collector toward the sun, $\dot{q}_{refl,coll_{right}}$ the reflected power flux toward the earth, $\dot{q}_{refl,coll_{side}}$ the reflected power flux from the side toward the space, $\dot{q}_{rad,coll_{left}}$ the power flux irradiated from the collectors toward the sun, $\dot{q}_{rad,coll_{right}}$ the power flux irradiated from them towards the earth, $\dot{q}_{rad,coll_{side}}$ the amount of power flux lost due to irradiation through the sides of the collectors, $\dot{q}_{PV}$ the power flux received by the photovoltaic panels, $\dot{q}_{antenna}$ the power flux received by the orbiting antenna beamed to the earth, $\dot{q}_{gs}$ the power flux received by the ground station and $\dot{q}_{user}$ the final power flux received by the user.

$$
\begin{cases}
\dot{q}_{sun} = \dot{q}_{abs,sat} + \dot{q}_{trasm,sat} + \dot{q}_{refl,sat} \\
\dot{q}_{trasm,sat} = \tau_{sat}\dot{q}_{sun} \\
\dot{q}_{refl,sat} = \dot{q}_{refl,sat_{left}} + \dot{q}_{refl,sat_{right}} + \dot{q}_{rad,sat_{side}} \\
\dot{q}_{refl,sat_{left}} = \rho_{sat,left}\,\dot{q}_{sun} \\
\dot{q}_{refl,sat_{right}} = \rho_{sat,right}\,(\dot{q}_{earth} + \dot{q}_{albedo}) \\
\dot{q}_{refl,sat_{side}} = \rho_{sat,side}\,\dot{q}_{space} \\
\dot{q}_{rad,sat_{left}}(t) = \varepsilon_{sat,left}\sigma_0\left|T^4_{sat,left}(t) - T^4_{space}\right| \\
\dot{q}_{rad,sat_{right}}(t) = \varepsilon_{sat,right}\sigma_0\left|T^4_{sat,right}(t) - T^4_{space}\right| \\
\dot{q}_{rad,sat_{side}}(t) = \varepsilon_{sat,side}\sigma_0\left|T^4_{sat,side}(t) - T^4_{space}\right| \\
\dot{q}_{abs,sat} = m_{sat}c_{p,sat}\left(T_{eq,sat} - T_{i,sat}\right) \\
\dot{q}_{reflector} = \eta_r\dot{q}_{refl,sat_{left}} \\
\dot{q}_{collector} = \eta_c\dot{q}_{reflector} \\
\dot{q}_{collector} = \dot{q}_{abs,coll} + \dot{q}_{trasm,coll} + \dot{q}_{refl,coll} \\
\dot{q}_{trasm,coll} = \tau_{coll}\dot{q}_{collector} \\
\dot{q}_{abs,coll} = \dot{q}_{rad,coll_{left}} + \dot{q}_{rad,coll_{right}} + \dot{q}_{rad,coll_{side}} \\
\dot{q}_{refl,coll} = \dot{q}_{refl,coll_{left}} + \dot{q}_{refl,coll_{right}} + \dot{q}_{refl,coll_{side}} \\
\dot{q}_{refl,coll_{left}} = \rho_{coll,left}\,\dot{q}_{sun} \\
\dot{q}_{refl,coll_{right}} = \rho_{coll,right}\,(\dot{q}_{collector} + \dot{q}_{earth} + \dot{q}_{albedo}) \\
\dot{q}_{refl,coll_{side}} = \rho_{coll,side}\,\dot{q}_{space} \\
\dot{q}_{rad,coll_{left}}(t) = \varepsilon_{coll,left}\sigma_0\left|T^4_{coll,left}(t) - T^4_{space}\right| \\
\dot{q}_{rad,coll_{right}}(t) = \varepsilon_{coll,right}\sigma_0\left|T^4_{coll,right}(t) - T^4_{space}\right| \\
\dot{q}_{rad,coll_{side}}(t) = \varepsilon_{coll,side}\sigma_0\left|T^4_{coll,side}(t) - T^4_{space}\right| \\
\dot{q}_{abs,coll} = m_{coll}c_{p,coll}\left(T_{eq,coll} - T_{i,coll}\right) \\
\dot{q}_{PV} = \eta_{PV}\dot{q}_{abs,coll} \\
\dot{q}_{antenna} = \eta_{DC,DC}\eta_{DC,RF}\eta_{a,e}\eta_{b,e}\dot{q}_{PV} \\
\dot{q}_{gs} = \eta_{gs}\eta_{at,e}\eta_{RF,DC}\eta_{DC,DC}C_{gs}\dot{q}_{antenna} \\
\dot{q}_{user} = \eta_{tr}\dot{q}_{gs}
\end{cases}
\tag{1}
$$

All these flow components are further defined by additional coefficients, including transmissivity, reflectivity, absorptivity, and the efficiencies associated with the several energy transformations between subsystems. More precisely, τ represents the amount of energy, which is transmitted across the surfaces, ρ the reflectivity of the surfaces, while the efficiencies are reported in the following table:

Table 1: Definition of the subsystem efficiencies

Variable	Component's Efficiency
η_r	Reflector
η_c	Collector
η_{PV}	Solar Cell
$\eta_{DC,DC}$	DC to DC Conversion
$\eta_{DC,RF}$	DC to RF Conversion
$\eta_{a,e}$	Antenna Emission
$\eta_{b,e}$	Antenna Beam Collection
$\eta_{at,e}$	Atmospheric Travel
η_{gs}	Rectenna Array Reception
$\eta_{RF,DC}$	RF to DC Conversion
C_{gs}	Rectenna Capacity Factor
η_{tr}	Wires Transmission

The model takes into consideration the efficiencies of each element of the system, indicated with the letter η, from the panel reflecting efficiencies to the line distribution from the ground stations to the final user. In this way the model can be more flexible and effective in representing the final power needed by the satellites to be beamed to the Earth. The final expression of Earth power consumption is formulated as follows:

$$P_{fin} = n\,\dot{q}_{sun} S_{sat}\,\eta_r\,\eta_c\,\eta_{PV}\,\eta^2{}_{DC,DC}\,\eta^2{}_{DC,RF}\,\eta_{a,e}\,\eta_{b,e}\,\eta_{at,e}\,\eta_{gs}\,\eta_{tr} C_{gs} = n\,\dot{q}_{sun} S_{sat} C_{gs} \prod_{i=1}^{m} \eta_i = \frac{n\,\dot{q}_{user} S_{sat}}{C_{gs} \prod_{i=1}^{m} \eta_i} \tag{2}$$

where n represents the total number of satellites needed by the system, S_{sat} the active surface of each satellite contributing to the power transmission (the mirrors' surface), η_i the efficiencies of each component of the global system and m the number of components considered. The formula points immediately out that the overall power production needed by the Solar Annular System is strongly affected by the efficiencies of the materials and components along the transmission line, the number of orbiting satellites around the Earth, mirror's surface and the final desired output for the user. As far as concerns the boundary conditions, in the examined problem there are basically two, one on the "hot" side of the satellite facing the sun and one on the "cold" side facing outer space and the Earth. The boundary condition on the cold end depends on the satellite's dispersed power flow toward the space and earth by radiation, while the related to the hot surface depends on the incoming power flow from the Sun and the dispersed irradiation. Both boundary conditions are time dependent, given that the satellites orbit around the Earth continuously, with different incoming power fluxes due to orbital corrections. To simplify the thermal physics of the satellites, it is assumed:

1) No reactions over the heated surfaces.
2) Constant thermal properties.
3) No internal energy production.
4) Only pure diffusion (no advection).

The governing thermal equation of each satellite's surface thermal response is therefore simplified as:

$$\frac{\partial T_{sat}}{\partial t} = k_{x,sat} \frac{\partial^2 T_{sat}}{\partial x^2} \tag{3}$$

where $k_{x,sat}$ represents the diffusion coefficient of the satellite along the sun – satellite direction, function of the thermal conductivity, density and specific heat of the selected material. The initial condition is instead the following one:

$$T_{sat}(x, t = 0) = T_i(x) = T_{space}(r_{orbit}) \tag{4}$$

where the initial temperature of the satellite is assumed to be equal to the temperature that an object has in the space near the considered orbit with radius r_{orbit}.
The boundary conditions on the "hot" face ($x = 0$) and on the "cold" face ($x = L_{sat}$) are respectively:

$$\frac{\delta T}{\delta x}(x = 0, t) = \frac{\dot{q}_{sun} - \dot{q}_{rad,sat_{left}}(t)}{\lambda_{sat}} \tag{5}$$

$$\frac{\delta T}{\delta x}(x = L_{sat}, t) = \frac{\dot{q}_{earth} + \dot{q}_{albedo} - \dot{q}_{rad,sat_{rigth}}(t)}{\lambda_{sat}} \tag{6}$$

where the right-hand side term of Eq. 5 represents the power flow entering the "hot" face of the satellite, while the right-hand side term of the Eq. 6 represents the power flow ingoing or outgoing from the "cold" face.

To simplify the analysis, the mirror body of the satellite is modelled as a sensitive disc with thickness L_{sat} and thermal conductivity λ_{sat}, since the main components are represented by the mirror surface and collector's one, which is simplified as a sensitive disc in the same way as reported in the above equations.

C. The Mathematical Solution

In order to solve the PDEs expressed in the equations reported in this analysis, it has been chosen to adopt the approximation technique based on a Finite Difference Method (FDM). The implemented scheme is the Explicit Euler Method and the mesh size along the discretized satellite's thickness is considered uniform and mono dimensional [33].

$$
\begin{cases}
T_{j,sat}^{i+1} = T_{j,sat}^{i} + k_{x,sat}\Delta t \frac{T_{j+1,sat}^{i} - 2T_{j,sat}^{i} + T_{j-1,sat}^{i}}{\Delta x^2} \\
T_{1,sat}^{i+1} = T_{2,sat}^{i+1} + \Delta x \frac{\dot{q}_{sun} - \dot{q}_{rad,sat_{left}}}{\lambda_{sat}} \\
T_{n,sat}^{i+1} = T_{n-1,sat}^{i+1} + \Delta x \frac{\dot{q}_{earth} + \dot{q}_{albedo} - \dot{q}_{rad,sat_{rigth}}}{\lambda_{sat}} \\
T_{j,sat}^{1} = T_{space}(r_{orbit}) \\
k_{x,sat} = \frac{\lambda_{sat}}{\rho_{sat} c_{p,sat}} \\
T_{j,coll}^{i+1} = T_{j,coll}^{i} + k_{x,coll}\Delta t \frac{T_{j+1,coll}^{i} - 2T_{j,coll}^{i} + T_{j-1,coll}^{i}}{\Delta x^2} \\
T_{1,coll}^{i+1} = T_{2,coll}^{i+1} + \Delta x \frac{\dot{q}_{collector} - \dot{q}_{rad,coll_{left}}}{\lambda_{coll}} \\
T_{n,coll}^{i+1} = T_{n-1,col}^{i+1} + \Delta x \frac{\dot{q}_{earth} + \dot{q}_{albedo} - \dot{q}_{rad,coll_{right}}}{\lambda_{coll}} \\
T_{j,coll}^{1} = T_{space}(r_{orbit}) \\
k_{x,coll} = \frac{\lambda_{coll}}{\rho_{coll} c_{p,coll}}
\end{cases}
\tag{7}
$$

The discretized form of the PDE system with the relative boundary and initial conditions is reported in Figure 7:

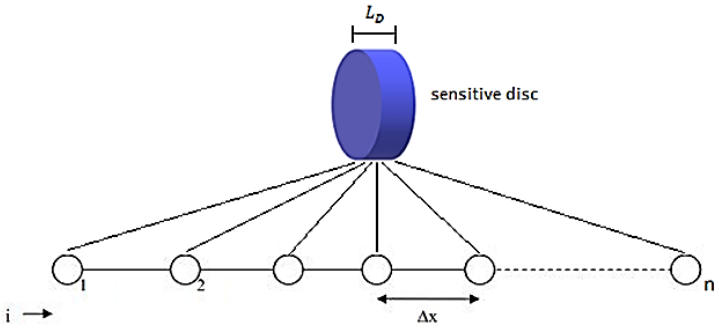


Fig. 7 Sensitive disc spatial discretization.

where each term of the governing system (Eq. 7) of the satellite's thermal response is now discretized in space through the index *i* and time through the index *j*. The expected thermal behavior of the heated panels should follow the response of a sensitive metal disc that has been heated by a pulsed CO_2 laser beam in laboratory and modeled through the system of equations implemented in this work. The plot below shows the experimental results compared to the simulated ones through the mathematical model of the tested sensitive disc, heated only by one side and left reaching thermal equilibrium in time.

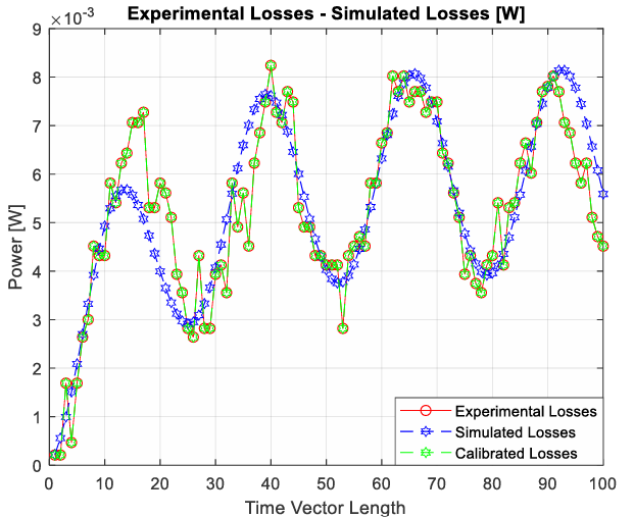


Fig. 8 Sensitive disc thermal behavior performed in laboratory and compared with the presented model.

The plot shows how the presented mathematical model has been validated, confirming its robustness and accuracy in predicting the thermal behavior of a sensitive disc even with a non-constant power input.

D. The System Model Simulator

The model implemented in Simulink has sequentially connected blocks that represent the different subsystems of the examined architecture, which are put together based on the principles of physics that govern the thermal interactions of the sun, the satellite, and the terrestrial ground section. As schematically shown in Figure 9, each subsystem is governed by functions that receive the input variables from the corresponding block, process them through corrective factors and conversions, and subsequently transmit the output of the subsystem to the subsequent subsystem as input. Additionally, the temperature value computed by the subsystem is cross verified with the temperature value derived from thermal simulation using Ansys, confirming that the discrepancy between the two values remains below a predetermined threshold to ensure high accuracy in the results. The model final output is compared to the user-defined desired output, which, as seen in Figure 9, is the power level received by the ground station under the *Desired Final Output* variable, located at the bottom of the model.

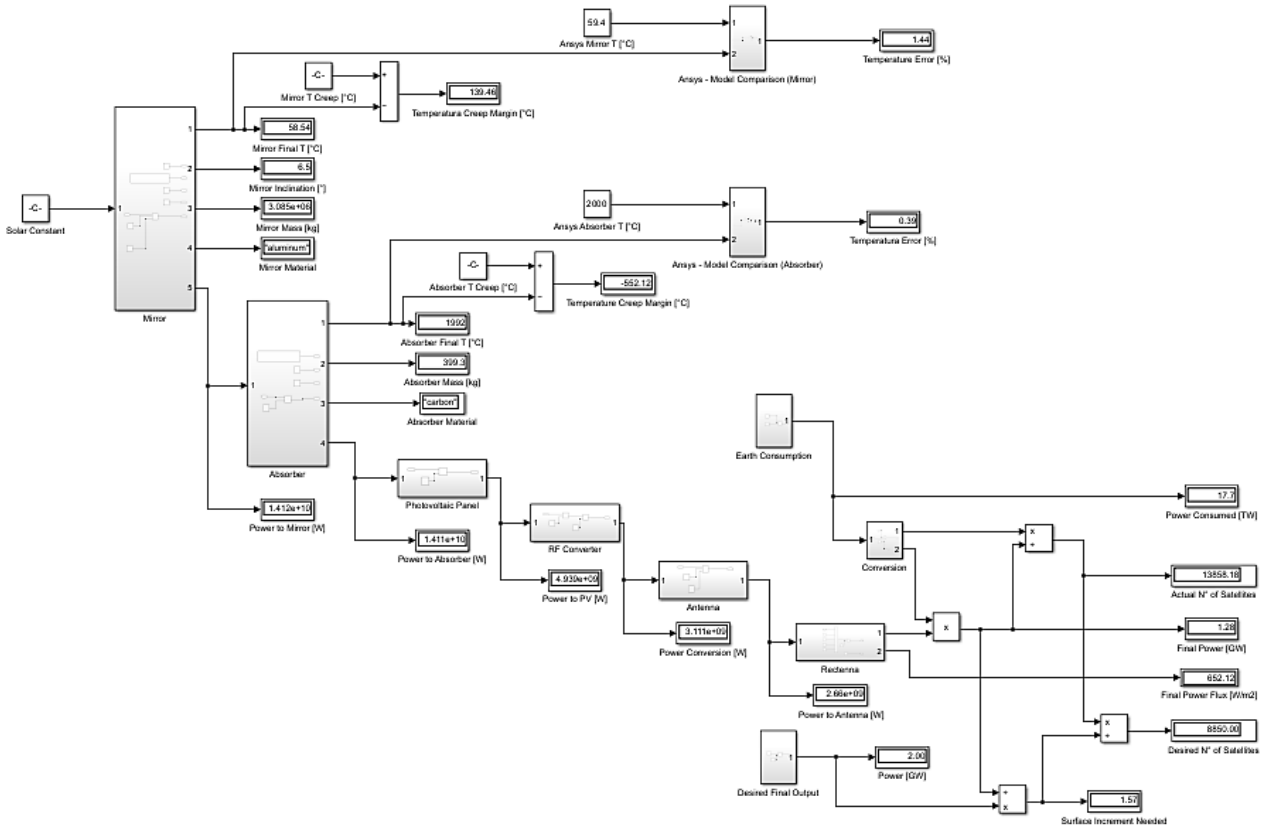


Fig. 9 Implemented Simulink block model.

A correction factor is then computed by comparing the output power with the nominal required power, which is then applied to the input data to calibrate the entire model for the specified power input fulfilment. The input values entered into the model, along with the output values obtained, will be shown in the final section of the Results.

IV. Optical, Thermal and Orbital 3D Simulations

A. Optical Simulation

The 3D CAD model used for both thermal and optical simulations is the one shown in Figure 5. Since it is not possible to recreate the 1:1 scale model on Ansys due to graphical and computational limitations, the model was scaled down in such a way as to lighten the simulations. The implemented scale is approximately 1:130000, so in order to estimate the size of the surfaces of the real architecture it is sufficient to multiply the dimensions of the 3D CAD model by the factor $1.6882*10^{10}$.

As shown in Figure 10, the model used to simulate the proposed satellite configuration from an optical and thermal perspective consists of the following components:

1) Radiative plate (in green, displayed on the right), whose function is to emulate the solar flux since it can be considered spatially constant
2) Radiative sensor (in the figure colored yellow and red), whose function is to map the solar flux to verify its spatial accuracy and homogeneous distribution
3) A second radiative sensor (in the figure in black) placed at the focal point of the two mirrors, whose function is to receive the concentrated radiation from the two mirrors and provide the area on which the radiative flux is collected
4) Two parabolic mirrors, which receive radiation from the source plate and concentrate it on the collectors initially placed at the focal distance of the parabolas, where the radiative sensor is also positioned to map the geometry of the flux

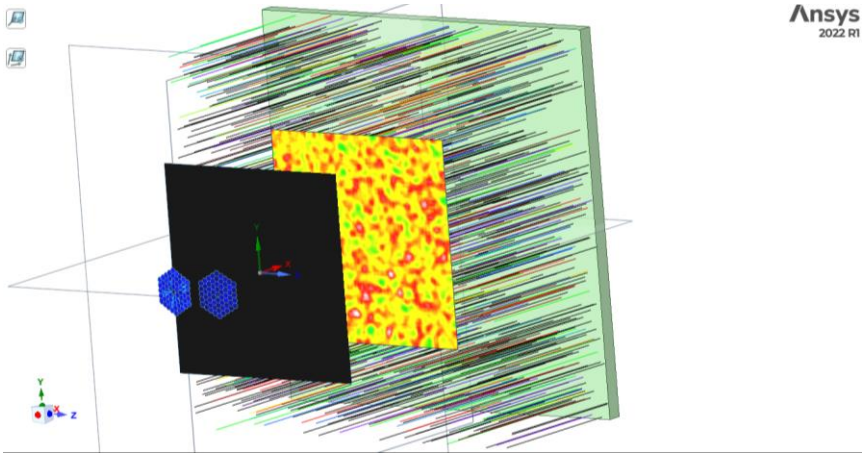


Fig. 10 Optical simulation of the system through Ansys Speos.

To reflect solar radiation onto the absorber in such a way that the absorber itself does not cast a shadow on the mirror surface, it is necessary to position the two absorbers facing the mirrors but shifted towards the symmetry axis of the satellite, so that the shadow of the two absorbing surfaces remains slightly outside the projection of the mirrors, ensuring the minimum necessary tilt of the surfaces.

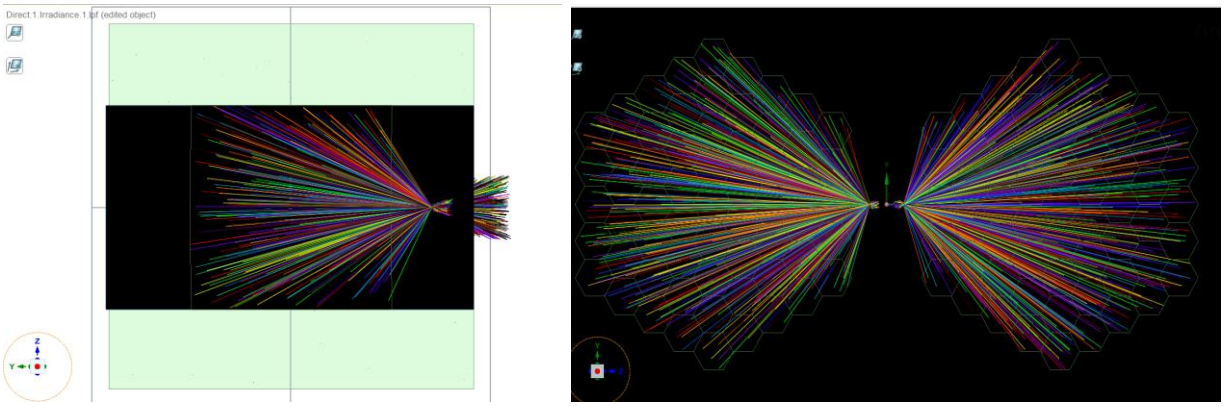


Fig. 11 Optical simulation of the solar radiation reflected and concentrated by the mirrors on the absorbers.

From a thermal perspective, the problem analyzed is governed by pure radiation, as the environment is represented by the portion of space near the geostationary orbit. The model does not account for conductive interaction between the bodies under consideration, since the mirrors and absorbers are separate entities spatially distanced from each other. Convection is absent.

Since solar radiation can be considered as a spatially constant field near the Earth and the simulated geostationary orbit, the surfaces in question can be appropriately scaled without altering the final results in terms of thermal response by the materials. In this way, it is possible to simulate the thermal response of the sensitive surfaces of the satellite without having to use large computational resources to recreate the model on a 1:1 scale.

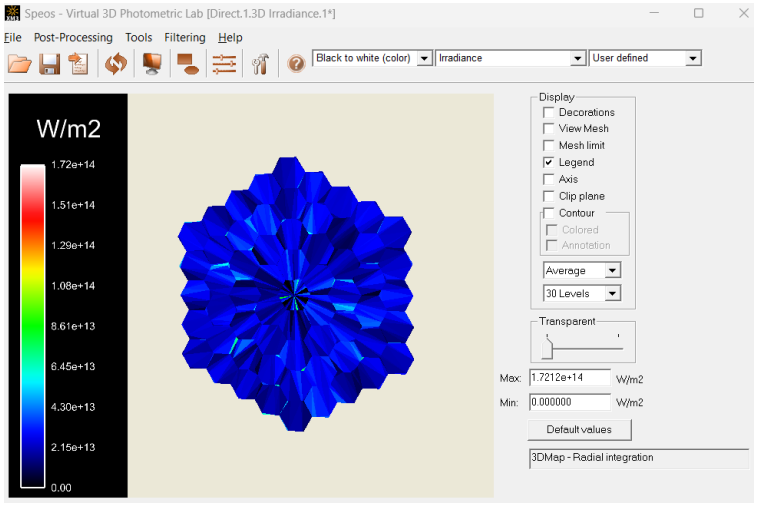


Fig. 12 Optical simulation of the power flux distribution over the mirror surface.

From Figure. 12, it can be seen that the average flux on the mirror is approximately $2.3*10^{13}$ W/m^2 (corresponding to the blue spectrum shown in the legend), a power value that is set on the source plate in order to correctly simulate the solar constant of 1367 W/m^2 in the scaled simulation. In fact, if the value of $2.3*10^{13}$ W/m^2 is divided by the previously mentioned scale factor of $1.6882*10^{10}$, the solar constant is thus obtained. The maximum recorded radiative flux from the optical simulation is instead $1.72*10^{14}$ W/m^2, located near the junctions of the hexagonal cells of the mirror, where the flux concentrates due to the discontinuities between the various hexagonal panels adopted.

Regarding the value of the radiative flux in the focal area where the absorbers are initially located, the simulations performed with Ansys Speos show that the maximum recorded flux is around $2.4*10^{17}$ W/m^2, as shown in Figure 13, while the average flux is found by appropriately delimiting the focal area drawn on the radiative sensor with an ellipse, in order to read the desired values with the *measure* function.

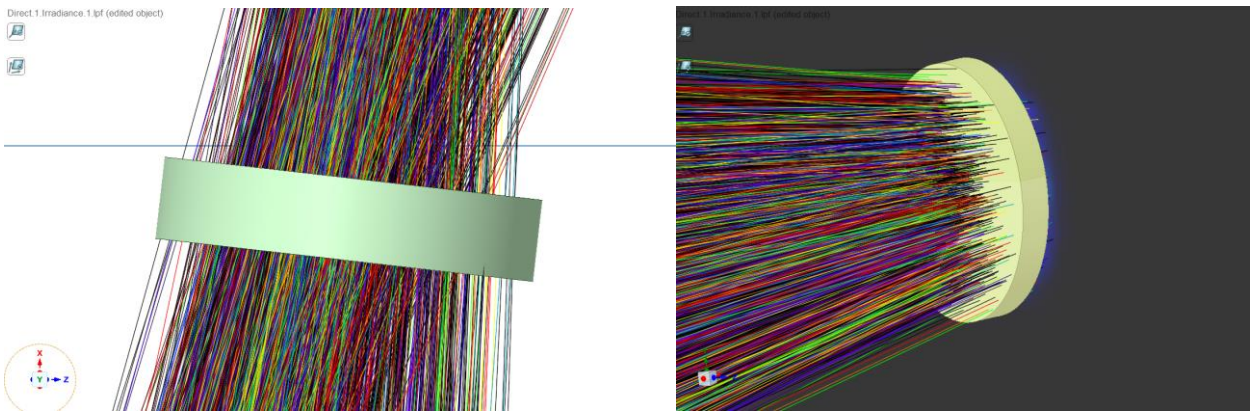


Fig. 13 Optical simulation of the ray tracking distribution over the absorber surface.

Figure 13 illustrates the elliptical absorber's capacity to capture all radiation focused by the mirror, thereby optimizing absorption efficiency while minimizing the absorber's surface area. In this way, the material employed for its construction is limited, thus contributing to keeping as light as possible the absorber's mass. Furthermore, the absorbers are rotated by 6.5°, aligning them parallel to the plane of the corresponding mirror. The concentrated radiation has no angle of incidence, resulting in reduced attenuation of the radiation. The average flux received by the surface of the absorber placed at the focus of the mirror is approximately $5.43*10^{16}$ W/m^2.

The total power received is $7.83*10^9$ W, which is equal to the total power received in the real case from a single mirror with an area of 5.74 km^2, reference value that is taken from previous calculations performed by NASA for the sizing of the RD1 architecture [34]. From this simple calculation, it is evident that the power levels resulting from the simulations match those of the 1:1 scale architecture, while the flux values require scaling to accurately represent the real flux. Since the area of the mirror in the simulation is 0.0003398 m², while the real area of one single mirror is 5.74 km², the ratio between the larger and smaller area determines the correction factor to be applied to the flow, which is the previously mentioned scaling factor $\aleph_{real/sim}$ $=1.6882*10^{10}$. Since the distance between the focus and the parabola scales linearly with the surface increase of the parabola, this corrective factor is well-defined to correctly scale the flow from the performed simulations to the real scenario.

To find the real average flux received by the absorber, it is sufficient to divide the average flux found through the simulation with Ansys Speos by the scaling factor ℵ, as reported below:

$$\dot{\bar{q}}_{abs,real} = \frac{\dot{\bar{q}}_{abs,SPEOS}}{\aleph_{real/sim}} = \frac{5.43247 * 10^{16}\ \frac{W}{m^2}}{1.6882 * 10^{10}} \cong 3217907\ \frac{W}{m^2} \tag{8}$$

A simple verification that can be carried out to confirm the validity of this result consists of dividing the total power received by one mirror, equal in both the simulated and real cases, by the scaling factor. This is mathematically possible due to the linear correlation that exists between the intensity of the radiative flux and the focal distance of the parabola. This verification is reported below, represented by the solution of the system:

$$\begin{cases} \dot{\bar{q}}_{abs,real} = \frac{\dot{\bar{q}}_{mir,REAL} S_{mir,REAL}}{\aleph_{real/sim}} = \frac{\dot{\bar{q}}_{mir,SPEOS} S_{mir,SPEOS}}{\aleph_{real/sim}} \\ \aleph_{real/sim} = \frac{S_{mir,REAL}}{S_{abs,REAL}} = \frac{S_{mir,SPEOS}}{S_{abs,SPEOS}} \end{cases}$$

$$\dot{\bar{q}}_{abs,real} = \frac{\dot{\bar{q}}_{mir,REAL} S_{mir,REAL}}{\aleph_{real/sim}} = \frac{1367\ \frac{W}{m^2} * 5.74 * 10^6\ m^2}{\frac{0.0003398\ m^2}{1.4 * 10^{-7}\ m^2}} \cong 3214920\ \frac{W}{m^2} \tag{9}$$

where the $S_{abs,SPEOS}$ refers to the surface area of the absorber in the scaled simulation, which is easily computed by dividing the total power $7.83*10^9$ W by the average flux $5.43*10^{16}$ W/m^2 received by the absorber. The value of the flow calculated in Eq. (9) and that estimated through Eq. 8 differs only by 0.093% due to the slight discrepancy between the manually calculated absorber area using the radiative map from the Ansys Speos radiative sensor and the actual absorber area calculated using the *Measure* function.

The power flow value reported in Eq. (9) and the solar constant will be used as input parameters for the Ansys Thermal simulations, to assess the thermal response and durability of the mirror and the absorber. The results will be then cross-checked with the ones computed by the mathematical model implemented in Simulink.

B. Thermal Simulation

The aim of the simulation performed with Ansys Thermal is to estimate the temperature values of the mirrors and absorbers, specifically the transient and final temperatures reached by the surfaces, ensuring they remain below the material's creep temperature. This limitation guarantees the preservation of mechanical properties during the operational phase, hence extending the materials' lifespan and the mission's duration. The estimated temperature is then compared to the one computed by the implemented mathematical model, validating its accuracy.

The geometry is imported directly from the prior optical simulation conducted with Ansys Speos; the antenna, the satellite's main body, and the supports are excluded from the calculation, as the simulation aims to assess the thermal response of the most stressed and critical surfaces. For the thermal simulation of the mirror, polished aluminum is chosen, since it is widely used in the aerospace field for its excellent reflective properties, low cost, and light weight. The important parameters to manually input into the Ansys simulation are the emissivity and reflectivity of the material, since these parameters are not included in the software's database. An emissivity of 0.1 and a reflectivity of 0.9 are thus introduced for the case of polished aluminum [35]. The optical properties of the selected material are also parameters that can be changed in the model, to enrich the database with more precise data derived from experimental tests. An automatically generated mesh is used: for this type of calculation, it is not necessary to adopt a particularly refined mesh since it is not a CFD analysis but a thermal-mechanical one. In the case of the first simulation, which is a steady-state type, a heat flux equal to 10% of the incident solar radiation, which corresponds to 136.7 W/m², is applied to the side of the mirror facing the Sun.

Since Ansys is not able to consider the optical properties of the material, the reflectivity of the component must be included by directly scaling the incident flux (the amount of radiation absorbed that contributes to the heating of the mirror). Furthermore, to complete the simulation in the steady-state case, it is necessary to add the losses due to radiation to the external environment (*radiation to ambient*), which is set to an arbitrary temperature of -160 °C (113 K) to simulate the conditions of space near Earth. However, this temperature does not significantly affect the simulation result since its contribution is raised to the fourth power according to the Stefan-Boltzmann law, thus representing a negligible contribution compared to the mirror's temperature. Such radiative loss is applied both on the face facing the Sun ("hot face") and on the opposite one ("cold face"). From the Ansys Thermal simulation, a final steady-state temperature equal to 59.26 °C is obtained for the mirror (Fig. 14), almost perfectly in line with the value of 59.10 °C computed through the implemented model - result of the discretized PDE's system previously reported in Eq. (9), with a deviation of 0.27%.

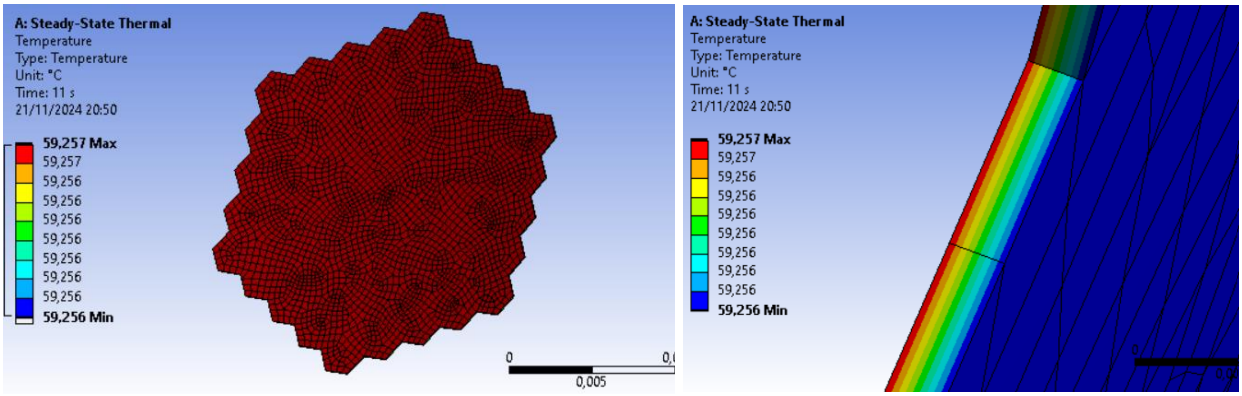


Fig. 14 Steady-state temperature of the mirror along hot and cold side.

As far as it concerns the absorber, the material that is selected for the thermal simulation is carbon-based, since it represents an optimal solution for high-temperature applications, especially if combined with photovoltaics panels [36], thanks to its thermal stability, corrosion resistance, lightness and low thermal expansion [37]. This surface is the most stressed among the entire satellite, since it must withstand heat flux which goes from hundreds of kW/m^2 to almost 1 MW/m^2. As previously shown in Eq. 8 and 9, the concentrated heat flux that reaches the focal area of the mirror is about 3.2 MW/m^2. If this value of heat flux is provided as input for the implemented model, a final steady-state temperature of 2034 °C is obtained for a graphite-based absorber. This temperature is far below the melting temperature of graphite, but the creep starting temperature for ceramic-based materials is about 0.4÷0.5 times the melting point [38], so in this case around 1440 °C. To guarantee the maximum durability of the absorber surface, it is therefore necessary to keep the final temperature of this component below the creep initial temperature. This thermal limit is satisfied with a heat flux not greater than 0.90 MW/m^2, which will bring the absorber to a final steady-state temperature of around 1402.3 °C on the hot face, thus acceptable for the operating scenario. The result of the simulation shows the final temperature of the absorber with an input heat flux of 0.90 MW/m^2, as reported in Fig. 15. In the case of the mirror, the creep starting temperature for aluminum is around 198 °C, so the final temperature reached by the mirror, 59.3 °C, is well below that limit, ensuring a longer lifespan for the mirrors too.

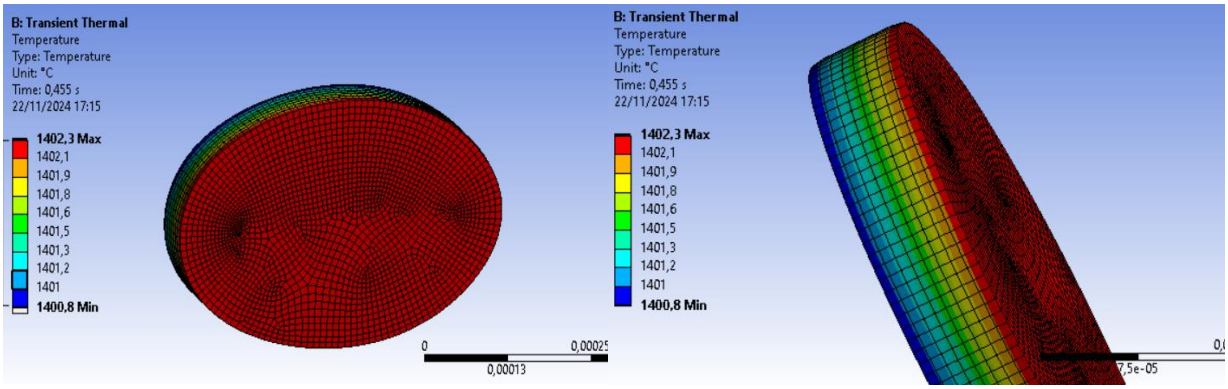


Fig. 15 Steady-state temperature of the absorber along hot and cold side.

The absorber final temperature computed through Ansys Thermal is therefore 1402.3 °C on the hot face, as shown in Figure 15, while the implemented model gives as result 1401.0 °C, thus a deviation of 0.093% from simulation and the model. To perform the transient regime simulations, Ansys Transient Thermal is used, which can import the simulation from Ansys Steady-State and starting from the previously set data. Below are shown the results from Ansys compared with the results of the simulations carried out using the implemented model, to demonstrate the overlap of the results and thus validate the accuracy of the model.

It is important to emphasize the significant difference in computational times between Ansys Thermal and the model implemented through code. Using an *i9* processor with 8 cores and 32 GB of RAM, it takes about 1 hour to simulate only the transient behavior of the mirror surface using 6 out of the 9 available cores. The time step set is 0.25 s, with a solar irradiation duration of 2500 s, and a mesh of approximately 9400 elements. Therefore, the number of iterations needed to complete the simulation on Ansys is:

$$n_{iter,ANSYS} = \frac{\Delta t_{sim} n_{elem}}{\Delta t_{step}} = \frac{2500\ s}{0.25\ s}\ 9400 = 9{,}400{,}000\ iterations \tag{10}$$

With the model implemented on Matlab instead, setting a time step of 0.00005 s for numerical stability reasons, for a simulation time of 2500 s of solar irradiation, and with 4 elements, the time taken by the computer is approximately 15 s. The number of iterations performed by the Matlab implemented model is the following one:

$$n_{iter,MODEL} = \frac{\Delta t_{sim} n_{elem}}{\Delta t_{step}} = \frac{2500\ s}{0.00005\ s}\ 4 = 200{,}000{,}000\ iterations \tag{11}$$

This clearly demonstrates that, with the same accuracy of the final result, the implemented model is much more computationally efficient compared to Ansys Thermal, and thus can be used to perform calculations and predictions on a variety of thermal scenarios and parameter combinations related to the presented configuration in a more scalable and faster way compared to dedicated 3D simulation software.

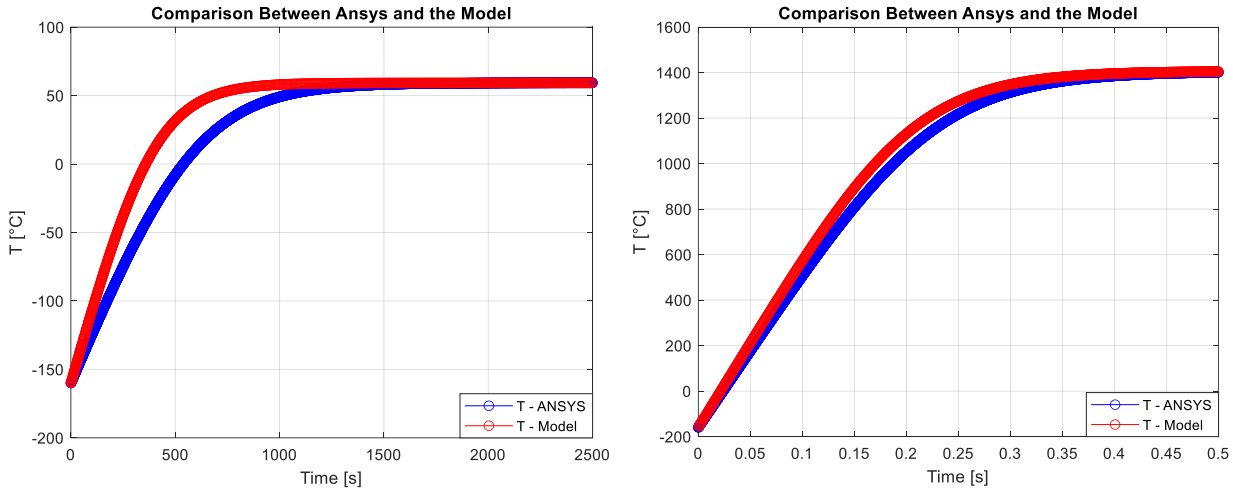


Fig. 16 Transient thermal profile comparison of the mirror (on the left) and absorber (on the right).

Finally, the plots shown in Figure 16 point out the difference between the thermal profile calculated with Ansys Thermal and the model implemented during the transient and steady-state regimes of the mirror and the absorber. It can be observed that in the case of the absorber, since the flux involved is very high, equal to 900,000 W/m², it takes about 0.5 seconds for the absorber to reach equilibrium temperature.

Whereas in the case of the mirror, given the lower thermal flux to be managed, equal to 1367 W/m², it takes much longer for the surface to reach thermal equilibrium, approximately 1500 s. A lower thermal flux means that the material will take longer to heat up, resulting in a longer transient period. Moreover, the material used for the mirror in this configuration is aluminum, which reflects 90% of the incident radiation, whereas in the case of the absorber, the material's reflection is practically negligible since carbon is used, so almost all of the incident radiation is absorbed, ensuring a faster radiative response compared to the mirror case, and thus a quicker transient.

C. A. Satellites Orbit Simulation

The objective of the orbital analysis and simulations performed on the proposed architecture is to determine the number of satellites, ground receiving stations, and the orbital configuration based on the initial problem parameters. The simulations are carried out by combining the Matlab *Satellite Communications Toolbox* with the implemented model, so that the model input and output data can be transferred to the appropriately modified toolbox and managed consequently. Furthermore, the model provides among its outputs an estimate of the size of the ground rectennas, based on the power beam generated in orbit by the satellite's antenna and its characteristics, which are also free parameters of the model. To estimate the diameter of the receiving rectenna, the satellite relative position above the rectenna must be analyzed. If an antenna is placed in geostationary orbit with a phase shift of 0° relative to its projection on Earth, a specific area of the rectenna on the ground is obtained, depending on the antenna's beam width, pointing accuracy, and diameter. If multiple satellites are supposed to be pointed at a single receiving rectenna, then it is necessary to calculate how the projection of the satellites varies over the area where the rectenna is located, to estimate how much it needs to be enlarged based on the total number of satellites connected to it.

The analysis carried on Ansys Speos and the simulator implemented on Matlab demonstrate how the diameter of the rectenna increases with the number of connected satellites, since the constellation of satellites are arranged with a certain angular distance from each other.

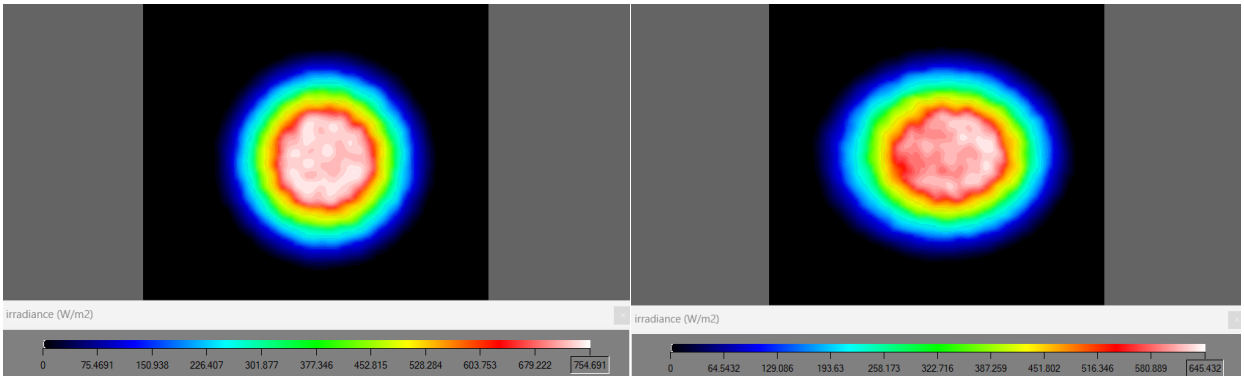


Fig. 17 Projection of the 0° (left) and 36.5° (right) tilted heat flux beamed by the orbiting antenna onto the ground rectenna.

As can be noted from a simple simulation performed on Ansys Speos to analyze the shift of the beam projection on the rectenna, reported in Figure 17, it can be observed that the focal area corresponding to the satellite inclined by 36.3° is larger (elliptical) compared to the projection of the satellite positioned at the zenith of the rectenna, which takes on a spherical shape. Since the area over which the flux is distributed increases with the increase in the satellite's inclination with respect to the rectenna's axis, the final flux will consequently be lower. In this tested configuration, a maximum flux of 645 W/m² at 36.3° is obtained, compared to 755 W/m² received by the rectenna at 0°.

Introducing into the mathematical model the projection of the beam generated by the orbiting antenna onto the ground rectenna as a function of its beamwidth, pointing accuracy, antenna diameter, and its tilt relative to the receiving rectenna, it is therefore possible to calculate the increase in the diameter of the rectenna as a function of the number of satellites pointing to it.

In Figure 18, the behavior of the rectenna's diameter and the received power flux are shown in the case of 1 to 1000 equally spaced satellites pointing at the same ground station. It can be observed from these plots that the diameter of the rectenna increases by almost 50% compared to the initial value, from 3940 m to 5735 m, in the case of 1000 satellites pointing at it. Regarding the power flux received on the ground, it increases from 164.3 W/m² to $6.1*10^5$ W/m², but such a flow would be unmanageable on the ground because the power density produced in a power beaming link may present safety risks for individuals, objects, and wildlife exposed to the beam. For both laser power beaming and RF power beaming, there are safety regulations for restricting continuous human exposure to particular power density levels, as determined by several organizations, including the IEEE [39] and ANSI [40].

After examining the behavior of rectenna sizes and the power flow received as a function of the orbital segment, it is now possible to estimate the requisite number of satellites to meet Earth's energy demand, their orbital positions, and the total number and location of the ground stations. The orbit considered in the simulations and orbital analyses is the geostationary orbit, since this particular configuration allows satellites to remain in the same position above the pointed rectenna, so there is no need for complex time dependent pointing and attitude control systems resulting from the variable ground track of the satellite during its revolution around the Earth.

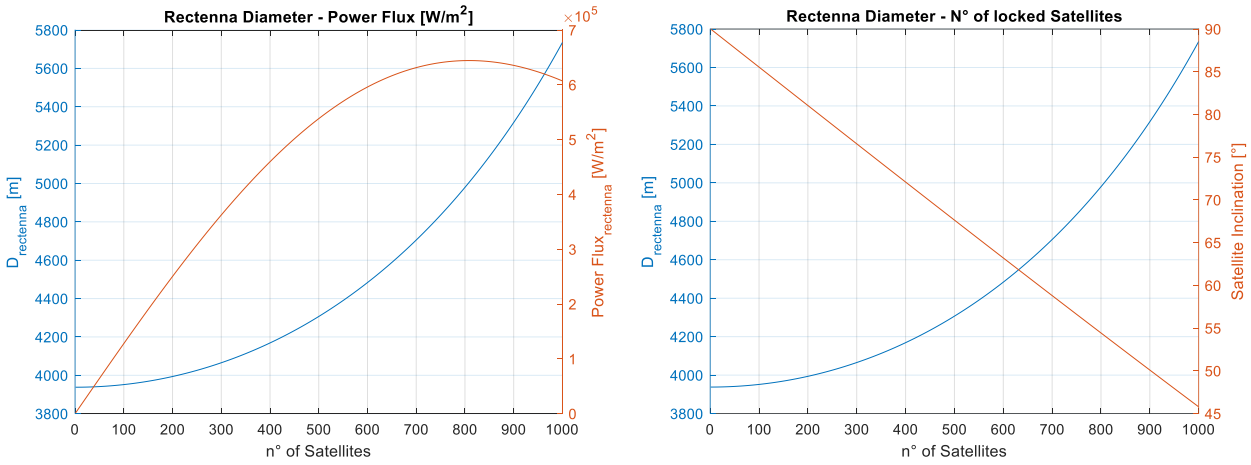


Fig. 18 Rectenna's diameter increment and Power Flux received as a function of number and inclination of satellites.

To arrange the satellites in orbit such that each satellite aligns with a rectenna on the ground, it is essential to construct a database collecting data for every country around the world, including population and per capita energy consumption. This method allows for the quantification of the power requirements of each state, hence enabling the estimation of the number of satellites needed by each state, based on the nominal power each satellite can deliver to the ground after considering all losses. The table comprising the population, consumption, and geographical coordinates of each country is constructed using the database from the *CIA website* [41], the worldwide population database from *World Population Review* [42], and *Geo Countries* [43] for the geographical coordinates. Upon completion of the database, it is incorporated as an input parameter into the developed model, allowing for updates with more recent statistical data to enhance the model's predictive accuracy.

Part of the database is provided below to illustrate the variables that will be included in the model for the orbital simulation conducted using the Matlab toolbox.

Country	Population	Latitude	Longitude	PowerConsumptioProCapita_W_
{'Afghanistan'}	39068979	34.52	69.2	151
{'Albania'}	2871954	41.33	19.83	1662
{'Algeria'}	44042091	36.78	3.05	1302
{'Angola'}	33451133	-8.08	13.23	278
{'Antigua e Barbuda'}	91.846	17.1	-61.85	3135
{'Arabia Saudita'}	30991207	24.62	46.72	8668
{'Argentina'}	45191965	-34.6	-58.45	2661
{'Armenia'}	2890893	40.18	44.5	1751
{'Australia'}	25743791	-31.93	115.33	9008
{'Austria'}	8921405	48.22	16.33	7292
{'Azerbaigian'}	10181730	40.38	49.86	1983
{'Bahamas'}	395.863	25.083	-77.35	4898
{'Bahrein'}	1483077	26.22	50.58	17349
{'Bangladesh'}	166298024	43.72	90.42	330
{'Barbados'}	281.698	13.01	-59.62	3361

Fig. 19 Partial view of the implemented world's geographical and power consumption database on Matlab.

To determine the required number of satellites to fulfill Earth's energy consumption, the overall power demand of the Earth must be divided by the nominal power output of the satellite. The total amount of terrestrial power is derived by adding up the power demands of each state (*PowerConsumptionProCapita* multiplied *Population* column), which, according to data from the aforementioned databases, is around 18.72 TW for 2022, consistent with the 2020 projection of 18.4 TW [44]. Subsequently, assuming a nominal power of 2 GW per satellite, accounting for losses, the total number of satellites required to meet the Earth's demand is 9360. If each satellite is pointed at one single ground station, then the total number of rectennas installed on ground corresponds to the number of satellites, totaling 9360 ground stations.

The number may be reduced if each rectenna could receive a higher power flow, although the limit imposed by regulations restricts the amount. Since the computational resources required for the orbital simulation of all 9360 satellites are very high, both in terms of GPU and RAM needed by the machine used, only one satellite and one rectenna are simulated for each country (the United States are divided into member states), for a total of 233 ground stations and a constellation of 233 satellites. Each satellite of the constellation is placed in a geostationary orbit, with a pointing inclination only in the direction of the Earth's latitude, and a longitudinal inclination of 0° relative to the associated ground station. So the satellite pointed at the ground station located in France, for example pointed at Paris, will have an inclination equal to the latitude of Paris, that is 48.87° N, and a longitude of 2.33° E. In this adopted configuration, the angle between the satellite and the ground rectenna is the lowest possible, thus the reception efficiency of the rectenna will reach the maximum value in the case of the selected orbit.

Below is the result of the orbital simulation carried out using the Matlab toolbox, suitably modified to retrieve the input and output data from the implemented model and the database created for accessing geographical data and power consumption. The 233 satellites that point at their respective rectennas on ground are capable of providing 466 GW of power to the Earth in this simulation, equivalent to 2.49% of the total terrestrial power consumption.

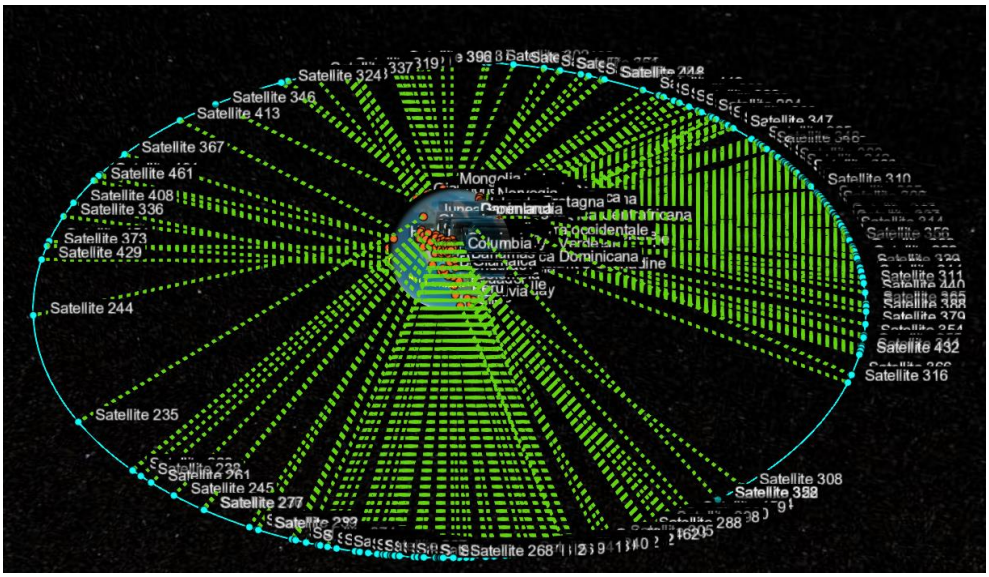


Fig. 20 Orbital simulation of the geostationary constellation of satellites, pointing at ground rectennas.

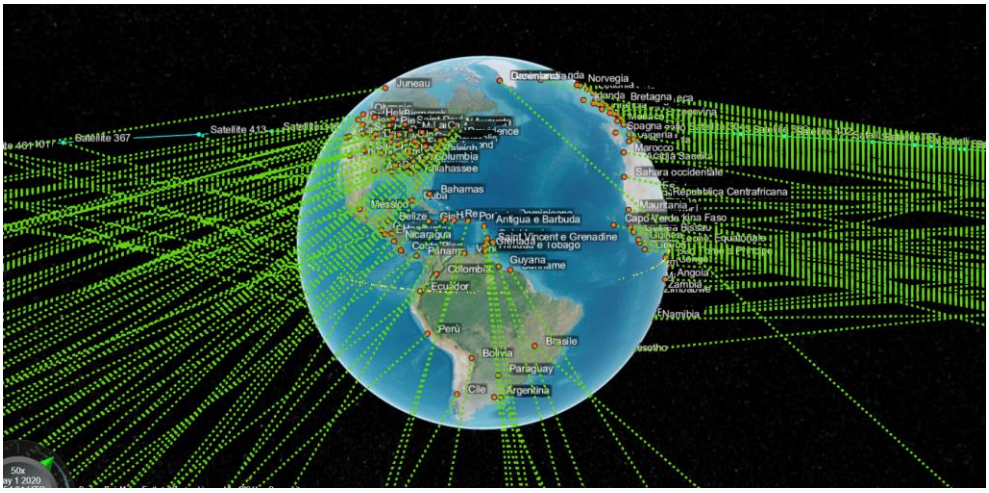


Fig. 21 Orbital simulation of the geostationary constellation of satellites (view of North and South America).

The number and geographical position of the 233 ground stations is shown on the map in Figure 22.

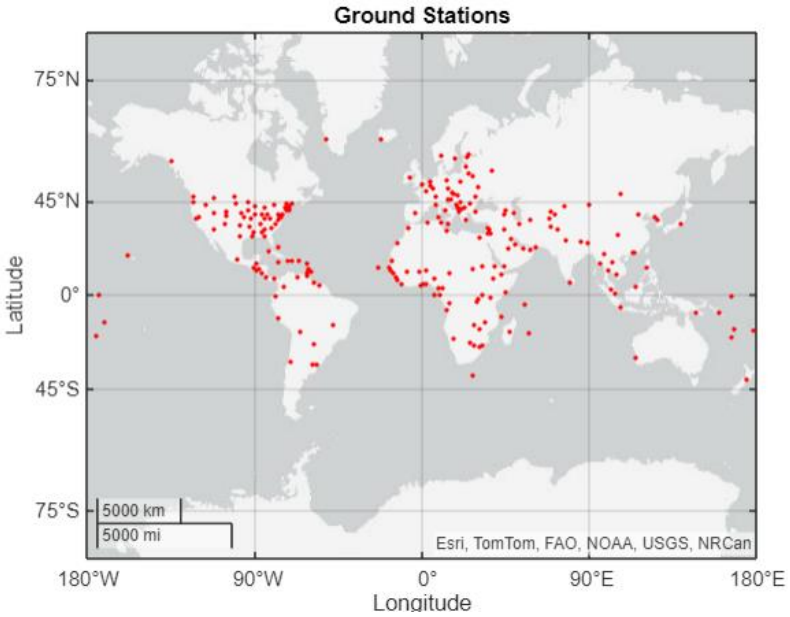


Fig. 22 Global map representation of 1 rectenna installed per country, totaling 233 rectennas.

V. Results

Before providing the numerical results of the implemented model, all input data used and integrated into the model are listed in the following table.

Table 2: Definition of input data

Variable	Variable Description	Value
I_s	Solar Constant	1367 [W/m^2]
P_E	Earth Power Consumption	18.72 [W]
P_{sat}	Satellite Nominal Power	2.0 [GW]
η_r	Mirror Reflectivity	0.90
η_c	Collector Absorptivity	0.99
η_{PV}	Solar Cell Efficiency	0.35
$\eta_{DC,DC}$	DC to DC Conversion Efficiency	0.90
$\eta_{DC,RF}$	DC to RF Conversion Efficiency	0.70
$\eta_{a,e}$	Antenna Emission Efficiency	0.90
$\eta_{b,e}$	Antenna Beam Collection Efficiency	0.95
$\eta_{at,e}$	Atmospheric Travel Efficiency	0.98
η_{gs}	Rectenna Array Reception Efficiency	0.78
$\eta_{RF,DC}$	RF to DC Conversion Efficiency	0.70
C_{gs}	Rectenna Capacity Factor	0.997
$\aleph_{real/sim}$	Scale Factor from Reality to Speos CAD	1.689*10^{10}
α_{beam}	Antenna Beam Angle	0.0001 [rad]
δ_{beam}	Antenna Beam Accuracy	0.00001 [rad]
$D_{antenna}$	Antenna Diameter	1596 [m]

Along with the data reported in Table 2, the thermal and optical properties of the materials used in the simulations are directly taken from the Ansys database (aluminum for the mirror and carbon for the absorber). The final parameter to be set before launching the simulation is the initial surface area of the mirror.

The model computes a final correction coefficient based on the initial value, considering the necessary adjustments to the starting area to achieve the specified power output of 2.0 GW delivered to the ground.

The initial value implemented for the mirror area is 11.473 km², a statistic derived straight from NASA's investigation for the RD1 architecture [34].

The following block scheme displays the outcomes of the simulation performed with the enhanced Simulink model, which is augmented by results from the simulations performed using Matlab, Ansys Speos and Ansys Thermal.

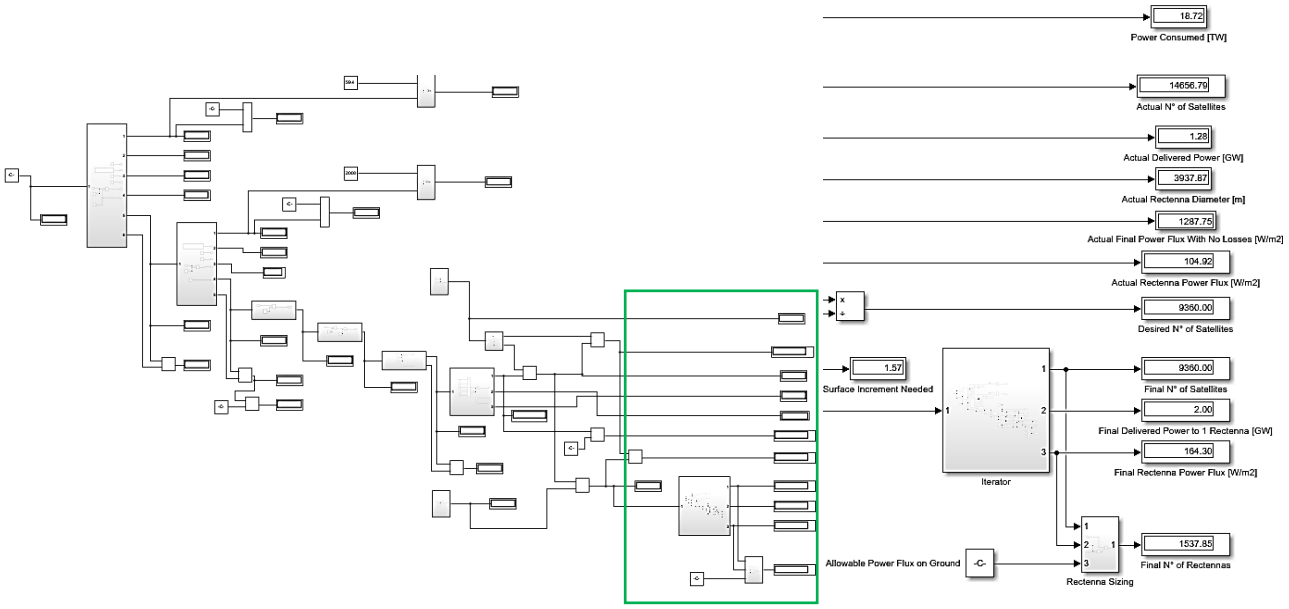


Fig. 23 The complete Simulink Model (on the left) and its final portion (on the right) displaying the outputs of the simulator.

The results indicate that the *Final Rectenna Power Flux* output value is 164.3 W/m², representing the power flow that the rectenna receives from the orbiting segment, already transformed into DC current and ready for distribution to end users.

This power flux value depends on the efficiencies of the entire system, but particularly on the size of the orbiting antenna, which determines the degree of power concentration, accuracy, and width of the beam achieved during the beaming phase directed towards the ground station.

Considering that in the hottest month of the year, the radiation that reaches the ground in the USA is about 240 W/m² as previously reported, and using the same conversion efficiency of the photovoltaic panel used in the proposed architecture, which is 35%, the final flux that the ground-based PV panel is able to handle is approximately 84 W/m². This value represents half of the power flux received by the rectenna in the performed simulation, which is 164.3 W/m². Therefore, the current simulated SBPS configuration, in terms of the final power flux delivered, is more efficient compared to a simple photovoltaic panel installed on the ground.

Increasing the size of the orbiting antenna would enable a narrower beam width, resulting in a more focused projection of the beam on Earth within a smaller area. Consequently, the ultimate flux received by the rectenna would be greater than the computed value, thereby reducing the rectenna's dimensions.

Whenever 6 satellites are pointed at each rectenna installed on the ground, for a total received power flux of about 1000 W/m^2 (equivalent to the maximum solar flux that can be recorded on a hot, cloudless day with optimal exposure on the ground), there would be a huge reduction in the total number of rectennas installed on the ground to meet the world's energy needs, totaling 1538 rectennas. Furthermore, 6 satellites pointing at the same rectenna would result in the rectenna being enlarged by a few meters, as previously shown in Figure 18.

To have a direct comparison with a terrestrial solar system, it is enough to compare the simulation result with the Noor Power Station installed near Ouarzazate in Morocco. This solar station can produce roughly 580 MW across an area of about $3*10^7$ m² [45], resulting in a power flux of approximately 17 W/m². The area covered by this solar station is equivalent to the area of approximately 2.46 rectennas, which are capable of generating about 4.92 GW of power, or 8.5 times the power generated by the Ouarzazate Power Station.

To conclude, the results of the Simulink model are briefly collected in the table below:

Table 3: Outputs of the implemented model

Variable	Variable Description	Value
n	N° of Satellites	9360
n_{gs}	N° of Rectennas	1538
$n_{sat,gs}$	N° of Satellites pointed at 1 Rectenna	6
P_{gs}	Power Received by 1 Rectenna	2.0 [GW]
$\dot{q}_{gs}$	Power Flux Received by 1 Satellite	164.3 [W/m^2]
$n_{sat,gs}\dot{q}_{gs}$	Power Flux Received by 6 Satellite	985.8 [W/m^2]
$\dot{q}_{lim}$	Max Power Flux by Regulations	1000 [W/m^2]
D_{gs}	Rectenna's Diameter	3940 [m]
S_{sat}	Satellite's Mirrors Surface	1.80*10^7 [m^2]
D_{sat}	Mirror Diameter	1694 [m]
L_{sat}	Mirror Thickness	0.07527 [mm]
m_{sat}	Mirror Mass	1.16*10^6 [kg]
$T_{eq,sat}$	Mirror Final Temperature	59.3 [°C]
S_{sat}	Satellite's Collector Surface	7859 [m^2]
D_{sat}	Collector Diameter	100 [m]
L_{sat}	Collector Thickness	0.07527 [mm]
m_{sat}	Collector Mass	399.3 [kg]
$T_{eq,sat}$	Collector Final Temperature	1401 [°C]
$\dot{q}_{coll}$	Collector Absorbed Power Flux	0.90 [MW/m^2]

VI. Final Considerations

Achieving Type 1 of technological level of civilization on the Kardashev Scale requires fulfilling the global energy demand, currently estimated to be approximately equal to 18.4 TW [44, 46]. The implemented model can size the overall dimension of the system in terms of number of satellites and ground stations around the Earth in such a way to cope with the power consumption of the Earth's population. From satellite data it is known that the Sun power flux reaching the Earth's orbit is about 1367 W/m^2 [47], so dividing the total terrestrial power requirement of 18.4 TW by this flux would give the rough estimate of the total surface of panels necessary to meet this demand from the theoretical point of view. Nevertheless, the whole system is governed by the efficiencies of many subsystems, which must be therefore considered both from a thermal and optical standpoint.

The model has been implemented for the sizing of a real system, so the equations reported are able to provide a more realistic estimate of the total surface area that the system must accomplish. The outputs of the simulations depend on a set of input parameters, which can be modified based on the assessed configuration, making the model flexible and capable of forecasting different scenarios from thermal, optical, and orbital points of view. All energy losses during the conversion among the various subsystems have been included to ensure that the obtained results are comparable in energy terms with solar systems already employed on ground, facilitating an evaluation of the actual effectiveness of a Space-Based Solar Power Satellite system.

The presented results do not suggest the existence of a singular configuration for fulfilling the Earth's energy demand; rather, the computed values identify the current quantifiable ranges of temperatures, power flows, sizing of primary components, and other essential engineering parameters that must be faced and overcome in order to implement a satellite system of such complexity.

Finally, the outputs of the mathematical implemented model show the thermal behavior of the satellites during the loading cycle, which assess the durability and performance of the materials adopted for the main components such as the panels and collectors.

Furthermore, the key point of the model is represented by its ability to simulate thermal transients and non-constant power sources in time, therefore the robustness and adaptability of the whole system can be assessed in case of pulsed or peak power fluxes from the sun or cosmic events.

References

[1] Dyson, F. J., "Search for Artificial Stellar Sources of Infrared Radiation", *Science*, Vol. 131, 1960, pp. 1667–1668.

[2] Wright, J. T., et al., "The Ĝ Infrared Search for Extraterrestrial Civilizations with Large Energy Supplies I: Background and Justification", *The Astrophysical Journal Supplement Series*, Vol. 217, No. 2, 2014.

[3] Matloff, G.L., *The Starflight Handbook: A Pioneer's Guide to Interstellar Travel*, Wiley, 2014.

[4] Badescu, V., "On the Dyson Sphere", *Acta Astronautica*, Vol. 46, No. 10–12, 2000, pp. 703–710.

[5] Niven L., *Ringworld*, Ballantine Books, 1970.

[6] Lacki, B. C., "Observational Prospects for Dyson Spheres", *Monthly Notices of the Royal Astronomical Society*, Vol. 484, No. 1, 2019, pp. 1183–1192.

[7] Zackrisson, E., et al., "Exoplanets and Stellar Astrophysics: Searches for Technosignatures from Advanced Civilizations", *The Astrophysical Journal Supplement Series*, Vol. 798, No. 2, 2015.

[8] Kardashev, N. S., "Transmission of Information by Extraterrestrial Civilizations", *Soviet Astronomy*, Vol. 8, No. 217, 1964.

[9] Nansen, R. A., "Microwave Wireless Power Transmission and Its Applications in Space-Based Solar Power Systems", *Journal of Energy Conversion and Management*, Vol. 45, No. 4, 2020, pp. 1207–1215.

[10] Brown, W. C., "The History of Power Transmission by Radio Waves", *IEEE Transactions on Microwave Theory and Techniques*, Vol. 40, No. 6, 1992, pp. 1239–1246.

[11] Glaser, P. E., "Power from the Sun: Its Future", *Science*, Vol. 162, 1968, pp. 857–861.

[12] Li, W., et al., "Development of China's Space Solar Power Research Program", *Acta Astronautica*, Vol. 128, 2016, pp. 1–9.

[13] Criswell, D. R., "Prospects for Space-Based Solar Power in Europe", *Acta Astronautica*, 2018, pp. 154, 33–42.

[14] Zhu, X., et al., "Long-Range Wireless Microwave Power Transmission: A Review of Recent Progress", *IEEE Journal of Emerging and Selected Topics in Power Electronics*, Vol. 9, No. 4, 2021, pp. 4932–4946.

[15] Shinohara, N., and Matsumoto, H., "Wireless Power Transmission Technologies for Solar Power Satellites", *IEEJ Transactions on Electrical and Electronic Engineering*, Vol. 8, No. 4, 2013, pp. 351–359.

[16] Maharjan, N., et al., "Atmospheric Effects on Satellite-Ground Free Space Uplink and Downlink Optical Transmissions", *Applied Sciences*, Vol. 12, No. 21, 2022.

[17] Glaser, P. E., "Power from the sun: Its future", Science, Vol. 162, pp. 867–886, 1968.

[18] DOE/NASA, "Program assessment report statement of finding Satellite power systems, concept development and evaluation program", DOE/ER-0085, 1980.

[19] Mihara, S., et al., "Microwave wireless power transmission demonstration on ground for SSPS'', *62nd Int. Astronaut. Congr.*, Cape Town, South Africa, IAC-11-C3.2.4, 2011.

[20] Sasaki, S., et al., "Microwave Power Transmission Technologies for Solar Power Satellites", *Proceedings of the IEEE*, Vol. 101, No. 6, 2011.

[21] Brown, W. C., "The History of the Development of the Rectenna", *Proceedings of the IEEE*, Vol. 80, No. 6, 1984, pp. 959–965.

[22] William, C. B., "Rectenna Technology Program: Ultra Light 2.45 GHz Rectenna and 20 GHz Rectenna", NASA-CR-179558, Rayhteon Company, 1987.

[23] Rodenbeck, C. T., et al., "Microwave and Millimeter Wave Power Beaming", *IEEE Journal of Microwaves*, 2020, pp. 229–259.

[24] Sengupta, M., et al., "The National Solar Radiation Data Base (NSRDB)", *Renewable and Sustainable Energy Reviews*, Vol. 89, 2018, pp. 51–60.

[25] Ongaro, F., and Summerer, L., "Peter Glaser lecture: Space and a sustainable 21st century energy system", *57th Int. Astronaut. Congr.*, Valencia, Spain, IAC-06-C3.1.01, 2006.

[26] de Groh, K. K, et al., "Environmental Durability Issues for Solar Power Systems in Low Earth Orbit", *International Solar Energy Conference*, Hawaii, 1995.

[27] Alan, T. C., *Fundamentals of Contamination Control*, SPIE Press, 2000.

[28] Mankins, J. C., "SPS-Alpha Mark-III and an Achievable Roadmap to Space Solar Power", *72nd International Astronautical Congress*, October 15, 2021.

[29] Artemis Innovation, Kobe University, FATE Consortium.

[30] Torchynska, T. V., and Polupan, G., "High efficiency solar cells for space applications", *Superficies y Vacío*, Vol. 17, No. 3, pp. 21–25, 2004.

[31] NASA Technology Transfer Program, "Advanced Efficiency Flexible Solar Film", LAR-TOPS-319.

[32] Kaushik, R., Satale, B., et al., "Space-Based Solar Power and Space Power", *Int. Journal of Electronics and Communications*.

[33] Prieto, F. U., Munoz, J. J. B., and Corvinos, L. G., "Application of the Generalized Finite-Difference Method to solve the Advection-Diffusion Equation", *Journal of Computational and Applied Mathematics*, Vol. 235, No. 7, 2011, pp. 1849–1855.

[34] Erica, R., et al., "Space-Based Solar Power", NASA Office of Technology, Policy, and Strategy, Report ID 20230018600, 2024.

[35] The Engineering ToolBox, "Surface Emissivity Coefficients", URL: https://www.engineeringtoolbox.com/emissivity-coefficients, 2003.

[36] Jena, A. K., et al., "Carbon-Based Materials for High-Performance Perovskite Solar Cells", *Chemical Reviews*, 2019.

[37] Mankins, T. M., "Thermal Design of Space Solar Power Systems", *Acta Astronautica*, 2014.

[38] Kim, M., and Kim, Y., "A Thermo-Mechanical Properties Evaluation of Multi-Directional Carbon/Carbon Composite Materials in Aerospace Applications", *Aerospace Journal*, 2022.

[39] "IEEE Standard for Safety Levels with Respect to Human Exposure to Electric, Magnetic, and Electromagnetic Fields, 0 Hz to 300 GHz", IEEE Std C95.1-2019, October 2019.

[40] "ANSI Z1 36 standards", The Laser Institute, 2017, URL: https://www.lia.org/resources/ laser-safety-information/laser-safety-standards/ansi-z136-standards [retrieved 25 June 2020].
[41] CIA.gov, "Country Comparisons – Energy Consumption per Capita", URL: https://www.cia.gov/the-world-factbook/field/energy-consumption-per-capita/country-comparison/ [retrieved 25 November 2024].
[42] World Population Review, "Total Population by Country 2024", URL: https://worldpopulationreview.com/countries [retrieved 25 November 2024].
[43] Geo Countries, "Country Geolocation", URL: http://www.geocountries.com/country/geolocation [retrieved 25 November 2024].
[44] Ritchie, H., Rosado, P., and Roser, M., "Energy Production and Consumption", *Journal: Our World in Data*, 2020.
[45] Power Technology, "Noor Ouarzazate Solar Complex", URL: https://www.power-technology.com/projects/noor-ouarzazate-solar-complex/ [retrieved 26 November 2024].
[46] IEA, "Electricity Information: Overview", URL: https://www.iea.org/reports/electricity-information-overview, License: CC BY 4.0, 2021 [retrieved 25 November 2024].
[47] Li, H., Lian, Y., Wang, X., Ma, W., and Zhao, L., "Solar Constant Values for Estimating Solar Radiation", *Energy*, Vol. 36, No. 3, 2011, pp. 1785–1789.